



**HAL**  
open science

## Anti-social cells: Predicting the influence of E-cadherin loss on the growth of epithelial cell populations

D. Walker, N.T. Georgopoulos, J. Southgate

### ► To cite this version:

D. Walker, N.T. Georgopoulos, J. Southgate. Anti-social cells: Predicting the influence of E-cadherin loss on the growth of epithelial cell populations. *Journal of Theoretical Biology*, 2009, 262 (3), pp.425. 10.1016/j.jtbi.2009.10.002 . hal-00554651

**HAL Id: hal-00554651**

**<https://hal.science/hal-00554651>**

Submitted on 11 Jan 2011

**HAL** is a multi-disciplinary open access archive for the deposit and dissemination of scientific research documents, whether they are published or not. The documents may come from teaching and research institutions in France or abroad, or from public or private research centers.

L'archive ouverte pluridisciplinaire **HAL**, est destinée au dépôt et à la diffusion de documents scientifiques de niveau recherche, publiés ou non, émanant des établissements d'enseignement et de recherche français ou étrangers, des laboratoires publics ou privés.

## Author's Accepted Manuscript

Anti-social cells: Predicting the influence of E-cadherin loss on the growth of epithelial cell populations

D. Walker, N.T. Georgopoulos, J. Southgate

PII: S0022-5193(09)00477-9  
DOI: doi:10.1016/j.jtbi.2009.10.002  
Reference: YJTBI5730



[www.elsevier.com/locate/jtbi](http://www.elsevier.com/locate/jtbi)

To appear in: *Journal of Theoretical Biology*

Received date: 17 February 2009  
Revised date: 5 October 2009  
Accepted date: 6 October 2009

Cite this article as: D. Walker, N.T. Georgopoulos and J. Southgate, Anti-social cells: Predicting the influence of E-cadherin loss on the growth of epithelial cell populations, *Journal of Theoretical Biology*, doi:[10.1016/j.jtbi.2009.10.002](https://doi.org/10.1016/j.jtbi.2009.10.002)

This is a PDF file of an unedited manuscript that has been accepted for publication. As a service to our customers we are providing this early version of the manuscript. The manuscript will undergo copyediting, typesetting, and review of the resulting galley proof before it is published in its final citable form. Please note that during the production process errors may be discovered which could affect the content, and all legal disclaimers that apply to the journal pertain.

# Anti-social cells: predicting the influence of E-cadherin loss on the growth of epithelial cell populations

***D Walker<sup>a\*</sup>, NT Georgopoulos<sup>b,§</sup>, J Southgate<sup>b</sup>***

*<sup>a</sup>Department of Computer Science, Kroto Institute, North Campus, Broad Lane,  
Sheffield S3 7HQ, U.K.*

*<sup>b</sup>Jack Birch Unit of Molecular Carcinogenesis, Department of Biology, University of  
York, York, YO10 5YW, U.K.*

*\*Corresponding Author: [d.c.walker@sheffield.ac.uk](mailto:d.c.walker@sheffield.ac.uk), Tel: +44 114 2221914, Fax: +44  
114 222 5945*

---

<sup>§</sup> Present address: Department of Chemical and Biological Sciences, School of Applied Sciences, University of Huddersfield, Huddersfield, HD1 3DH.

**Abstract**— The characteristics of biological tissues are determined by the interactions of large numbers of autonomous cells. These interactions can be mediated remotely by diffusive biochemical factors, or by direct cell-cell contact. E-cadherin is a protein expressed on the surface of normal epithelial cells that plays a key role in mediating intercellular adhesion via calcium-dependent homotypic interactions. E-cadherin is a metastasis-suppressor protein and its loss of function is associated with malignant progression.

The purpose of this study was to apply an agent-based simulation paradigm in order to examine the emergent growth properties of mixed populations consisting of normal and E-cadherin defective cells in monolayer cell culture. Specifically, we have investigated the dynamics of normal cell:cell interactions in terms of intercellular adhesion and migration, and have used a simplified rule to represent the concepts of juxtacrine Epidermal Growth Factor Receptor (EGFR) activation and subsequent effect on cell proliferation. This cellular level control determines the overall population growth in a simulated experiment.

Our approach provides a tool for modeling the development of defined biological abnormalities in epithelial and other biological tissues, raising novel predictions for future experimental testing. The results predict that even a relatively small number of abnormal ('anti-social') cells can modify the rate of the total population expansion, but the magnitude of this effect also depends on the extrinsic (culture) environment. In addition to directly influencing population dynamics, 'anti-social' cells can also disrupt the behavior of the normal cells around them.

**Keywords**—Agent-based computational model, epithelial cells, E-cadherin, intercellular adhesion

## 1. INTRODUCTION

The development of normal tissue architecture is critically dependent on the ability of individual cells to form stable adhesive contacts. In many tissue types, contacts are mediated by cadherins, a family of transmembrane proteins that mediate intercellular adhesion via interactions with homotypic proteins on opposing cell surfaces. Epithelial tissues express the cadherin subgroup E-cadherin, which is critical for forming initial adherens contacts between cells in developing tissues or cell cultures, allowing more established structures, such as tight junctions and desmosomes, to develop. In order to assume a functional conformation, E-cadherin requires the presence of extracellular calcium ions, with a concentration of  $>1\text{mM}$  required for the formation of stable contacts (Southgate et al., 1994; Baumgartner et al., 2000). This gives rise to the paradigm that below a concentration of  $1\text{mM}$ , E-cadherin is extrinsically non-functional, but becomes functional as the calcium concentration nears physiological ( $2\text{mM}$ ), which may be exploited experimentally.

Loss of E-cadherin function is associated with a reduction in tissue integrity and loss of normal architecture and function. Mutation or epigenetic silencing of the E-cadherin gene have been associated with malignant transformation and invasive behaviour (Foty and Steinberg, 1997; Conacci-Sorrell et al., 2002; Steinberg et al., 2008), whilst increasing the expression of functional E-cadherin has been shown to reduce the growth of malignant cell lines in a reconstituted extracellular matrix (Foty and Steinberg, 2004).

In addition to providing mechanical integrity to a growing cell population, E-cadherin also plays an important role in growth regulation. The concept of contact-inhibition of growth by stable intercellular contacts is well accepted. Although the mechanisms are not yet fully understood, one supported hypothesis is that sequestration of the transcription factor  $\beta$ -catenin to intercellular contacts leads to the loss of a pro-proliferative mediator (Stockinger et al., 2001).

However, there is growing evidence that cell contact may also positively influence cell growth, at least in the early stages of tissue formation (Nelson and Chen, 2002; Liu et al., 2006). Both positive (Pece and Gutkind, 2000) and negative (Takahashi and Suzuki, 1996) interactions between E-cadherin and the Epidermal Growth Factor Receptor (EGFR) have been reported, as well as the indirect activation by intercellular contact of a number of intracellular signaling molecules including Rac1 (Liu et al., 2006), Akt-PkB (Pece et al., 1999) and the cyclin-dependent kinase inhibitor, p27 (St Croix et al., 1998).

The aim of the study presented here was to use computational simulation to explore the potential effects of loss of E-cadherin function (representing ‘anti-social’ cell behaviour) on the growth characteristics of otherwise normal epithelial cell populations. In particular, we were interested in whether loss of function from a relatively small subset of a cell population would have a discernable effect on the total population growth dynamics and whether the aberrant population would be expected to influence the growth of the normal population, or vice versa.

Traditionally, computational models are based on mathematical equations that represent the averaged behaviour of a large number of individuals. However, in order to model mixed cell populations, and to resolve interactions at the level of individual cells, it is necessary to adopt a modeling paradigm that can inherently represent discrete individuals and their interactions. We have previously described Epitheliome, a software agent-based model of epithelial cells that has been used to simulate tissue growth (Walker et al., 2004a) and wound healing (Walker et al., 2004b) in monolayer cell cultures. The model consisted of a population of ‘seeded’ virtual cells, or software agents, placed in a specified virtual environment and allowed to interact according to pre-programmed rules representing cell cycle progression (represented by increment of an internal clock), quiescence and division, intercellular adhesion, changes in morphology, migration and simple physical interactions. Each software agent executes these rules according only to its current internal state and interaction with its immediate environment (both extracellular factors and adjacent cells). There is no concept of overarching control in the model, thus model

simulations produce *emergent* behaviour that arises solely from the behaviour and interactions evolving at a cellular level. During the previous decade, the agent- or individual- based paradigm has been applied to representing cellular interactions, with examples including tumour growth (Anderson and Chaplain, 1998; Mansury et al., 2002; Drasdo and Hoeme, 2005), immune-vascular cell interactions (Folcik et al., 2007; Tang et al., 2007) and angiogenesis (Bentley et al., 2007).

Previously, we described our prototype agent model of epithelial cell monolayer growth and compared the simulation results with *in vitro* population growth assays (Walker et al., 2004a) performed on cultured normal human urothelial (bladder epithelial) cells (Southgate et al., 1994). Our previous results (Walker et al., 2004a) and also more recent experimental data based on actual cell counts (see figure 1), showed an unexpected enhancement in population growth rate in physiological calcium concentrations. This was surprising and counter-intuitive with respect to the known growth inhibitory effects of stable intercellular contacts described above. This *in vitro/in silico* comparison prompted a subsequent computational exploration of potential biological mechanisms contributing to this unexpected behaviour. We recently used a multi-scale agent/signaling model to demonstrate that enhanced proliferation in sub-confluent cultures may be mediated by the juxtacrine engagement of the EGFR at intercellular contacts, resulting in sustained downstream activation of cytoplasmic Extracellular signal-regulated kinase (Erk) (Walker et al., 2008). It has been reported that Erk activation sustained for several hours in G1 is required for cell cycle progression (Roovers and Assoian, 2000; Yamamoto et al., 2006). We have incorporated a new rule into our agent model to represent the concept of *positive* mediation of growth associated with increased intercellular contact. In particular, we enforced the requirement that a cell must have maintained intercellular contact for a minimum period of time during the early G1 phase (arbitrarily set to 4 hours) in order to become proliferative (exit G0). It is not stipulated that this contact must relate to the persistence of a single stable contact, but could potentially arise from a series of transient contacts formed during cell migration.

In our previous publication (Walker et al., 2008), we explored the concept of the emergence of phenotypic heterogeneity within genetically homogeneous cell communities – in particular, how random migration and contact formation could result in vastly differing intracellular Erk activation levels within individual cells, which are not observed when protein expression is visualized on a population level (e.g. by western blotting). In the study described here, we focused on cellular and population level effects arising within heterogeneous communities.

We describe how we have applied our agent-based model of epithelial cell growth to explore the effect of the mutation of a single gene that results in the loss of E-cadherin function amongst a variable subset of cells, on the nature and dynamics of population growth in monolayer cell culture. This dysregulated rule set represents how one aspect of malignant transformation and hence interactions and influence on a population of normal cells, may be expected to give a novel insight into neoplastic growth and malignant progression processes. Whereas the interactions between normal cells are homeostatic and regulatory of the cellular community (i.e. “social” interactions), we have termed the behaviour of the modified cells as “anti-social”. We have chosen to use a monolayer-based simulation, as this allows direct comparison with *in vitro* experiments where the distribution of E-cadherin can be visualized, thus providing a route for model validation.

## 2. MODELLING METHODOLOGY

A full description of the current model, based on the standardised description protocol suggested by Grimm et al., (2006) is given below.

### 2.1 Purpose

The agent-based model we have employed in this study is based on an extended version of that described in our previous publications (Walker et al., 2004a; Walker et al., 2004b). The purpose of this model is to explore the effect of a mutated gene controlling intercellular adhesion in a proportion of the population on i) interactions between agents ii) the adoption of a particular

phenotype (e.g. migratory, quiescent) amongst subsets of agents and iii) the emergent population dynamics. We were particularly interested in the interaction of ‘mixed’ populations of agents e.g. those consisting of both cells containing the normal (henceforth referred to as EC-N, or E-cadherin-normal) cells and mutated gene (EC-A, or E-cadherin abnormal) cells.

The primary global emergent behaviour produced by this model is the population dynamics i.e. the total number of agents as a function of simulation time. The foundation of this behaviour is the individual interactions between agents, which initially may come into contact at low to moderate densities as a result of random migratory behaviour. These interactions may lead to stable or transient adhesions (again, stochastically-based) which in turn affect subsequent migration and proliferation/quiescence.

## 2.2 State variables and scales

Agents in the model represented individual urothelial cells placed on a  $1\text{mm}^2$  substrate containing a fixed, uniform concentration of exogenous calcium ions. Spatial units are measured in  $\mu\text{m}$  and each model iteration represents 30 minutes of real time. The model is 2.5 dimensional – interactions occur only in the x-y plane, but each cell is considered as an oblate spheroid with a variable “height” in the z plane. This allows a cell to alter its morphology, whilst maintaining a fixed volume.

Agent memory parameters relevant to this particular computational exploration include:

- Unique identification number for every cell
- Current cell cycle phase and position within phase, or flag representing quiescent state
- Cell radius (may differ between xy and z planes)
- Current migration direction
- Number and size of stable (E-cadherin-mediated) intercellular adhesions, and the identification flags of those cells with which adhesions are shared
- Number of current transient (non E-cadherin-mediated) interactions with adjacent cells

- Endogenous expression of E-Cadherin protein (=1 for “normal” (EC-N) or 0.01 for “abnormal” (EC-A) cells, respectively)

### 2.3 Process overview and scheduling

The model is incremented in fixed time steps according to the order shown in figure 2. Model parameters are scaled so that each agent iteration represents a period equivalent to 30 minutes. Following the memory update of every agent according to the rules described below, a numerical algorithm is used to eliminate or minimise cell overlap that has arisen due to cell growth, division and migration. This sub-model runs for a maximum of 200 iterations (empirically determined to be sufficient to achieve equilibrium in relatively high agent densities) and returns new positional information to the agent model. It should be noted that the purpose of this algorithm is to eliminate overlap only, and the concepts of *active* cell migration and adhesion are dealt with entirely within the agent model. Further details of this algorithm can be found in section 2.5.5.

### 2.4 Initialisation and data recorded

The starting point for each simulation was 200 “seeded” cells, each with endogenous E-cadherin expression set to either 1 (normal, or EC-N) or 0.01 (aberrant, or EC-A), randomly placed on a  $1\text{mm}^2$  substrate. The non-zero value for EC-A cells reflects the fact that experimentally, genetically-modified cells were observed to express small amounts of E-cadherin protein, though very little was localised to cell membranes compared to normal urothelial cells. The ratios of EC-N and EC-A cells for each model run is given in Table 1. In the case of mixed populations, individual agents were randomly assigned to express normal or reduced E-cadherin amounts (i.e. randomly allocated to the EC-N or EC-A category). This intrinsic or endogenous expression associated with each agent would later be converted in to an *active* E-cadherin expression value, depending on the exogenous calcium concentration in the cell adhesion rule, as described below. Following cell division, each daughter inherited the endogenous E-cadherin protein value of the parent cell.

Simulation number	% EC-N	% EC-A
1	100	0
2	90	10
3	75	25
4	50	50
5	25	75
6	0	100

**Table 1 List of EC-N and EC-A starting population fractions associated with each simulation set**

All ‘seeded’ cells were initialised in G0, representing a confluent, growth-arrested population following harvest and re-seeding onto a fresh substrate. For each simulation, the exogenous calcium concentration was set to a fixed value which could be accessed by the agents at any time. It did not vary spatially and remained constant throughout the simulation. All simulations were carried out in both low (0.09mM) virtual exogenous calcium concentrations (where endogenous E-cadherin is generally not functional) and physiological (2.0mM) calcium (where endogenous E-cadherin will function to form adherens junctions). Hence a distinction was made between *extrinsically* non-functional E-cadherin (due to the influence of environmental factors on the ability of normally expressed protein to interact effectively) or *intrinsically* non-functional E-cadherin (representing a mutation or loss at the epigenetic level).

For each set of initial conditions, three simulations were run for 225 iterations, representing approximately 4 3/4 days of real cell growth. Agent locations and total agent numbers, as well as a summary of a selection of more detailed data (e.g. numbers of cells migrating, entering or leaving G0 and details of stable intercellular contacts) were stored at each iteration.

All standard simulations were carried out using the Matlab software package (The Mathworks Inc., [www.mathworks.com](http://www.mathworks.com)). Larger simulations to check boundary sensitivity (see section 2.6)

were carried out using our in-house C-based agent modelling platform FLAME (<http://www.flame.ac.uk/>) using an identical rule set and protocol.

## 2.5 Sub-Models

Each of the following rule sets is summarised in a pseudo-code form in boxes 1-4. All key model parameters associated with each rule are given in table 2.

### 2.5.1 Intercellular Bonding/Contact behaviour

This rule is summarised in box 1. At every model iteration, an agent will have the opportunity to form stable intercellular contacts with up to a maximum of 6 adjacent neighbours with edges within 5 $\mu$ m (estimated as the length of maximum lamellapodia extension from time-lapse microscopy images). Agents may also form transient contacts with up to 6 neighbours within the same distance constraint. Close inspection of time-lapse microscopy images of NHU cells cultured in low calcium medium (e.g figure 3) revealed that cells tended to remain in contact with one another for periods of up to one hour, before migrating away to form new contacts. These transient contacts are not stabilized by E-cadherin, but could be the result of weak interactions mediated by inter-membrane surface tension, as implied by immunofluorescence microscopy (see Southgate et al., (1994)).

The functional E-Cadherin amount of a given agent,  $P_m$ , is calculated according to the endogenous E-cadherin amount,  $E_m$ , and exogenous calcium concentration,  $X$ , as follows:

$$P_m = E * \left[ A + \frac{C}{(1 + T e^{-B(X-M)})^{\frac{1}{T}}} \right] \quad (1)$$

where A=lower asymptote (= 0.1), C=upper asymptote (=0.57), M=point of maximum gradient (=1mM), B=growth rate (=1), T determines the relationship between maximum gradient and asymptotes (=10) and X is the exogenous calcium concentration in mM.

The decision for a pair of agents to form a stable (E-Cadherin-mediated) contact is stochastic, based on the following equation for bond formation probability,  $BP_{mn}$ :

$$BP_{mn} = \frac{\sqrt{(P_m * P_n)}}{(esep_{mn} + 1)^q} \quad (2)$$

Where  $P_m$  and  $P_n$  are the functional E-cadherin levels of agents  $m$  and  $n$ ,  $esep_{mn}$  is the distance between the edges of the cells in  $\mu\text{m}$  and the exponent parameter  $q=1/3$  (estimated). The pair of cells will form an initial E-cadherin mediated contact if a pseudo-random number is less than  $BP_{mn}$ .

Although phenomenological in nature, the form of this rule results in a relationship between BP and exogenous calcium that closely mirrors the relationship between binding activity and calcium reported in Baumgartner et al., (2000). For a pair of agents with normal endogenous E-cadherin expression, this implies that formation of a stable contact is significantly higher in physiological calcium concentrations, than for concentrations less than 1mM.

Any pair of cells within  $5\mu\text{m}$  that have not already formed a stable contact according to the rule described above, interact transiently. In order to incorporate the concept that cells with a larger mutual contact would experience a larger attractive force, and therefore be likely to remain in contact for longer, we included the rule that for cells with edge separation,  $esep_{mn}$ , less than  $5\mu\text{m}$ , the mutual contact length,  $clen_{mn}$ , is given by:

$$clen_{mn} = \frac{(\max\_sep - esep_{mn}) * p * \max\_r_{mn}}{\max\_sep} \quad (3)$$

where  $\max\_sep$  is the maximum separation distance at which cells can form an initial contact (estimated as  $5\mu\text{m}$ ),  $\max\_r_{mn}$  is the radius of the larger of the two cells in contact, and  $p$  is a dimensionless constant linking this radius to the size of the contact formed (estimated to have a value of 1.5 from observation of time-lapse microscopy images of the interactions of urothelial cells in culture). For the case that  $esep \leq 0$  (cells touching or forced together by high local population density)  $clen_{mn} = 1.5 \times \max\_r_{mn}$ .

**BOX 1 - Adhesion Rule****1. Stable (E-cadherin-mediated) adhesion**

*If number\_stable\_bonds < 6*

*Calculate functional Ecad level  $P_m$  (eq 1)*

*Find separation to all neighbours within  $5\mu\text{m}$*

*For each non-bonded neighbour*

*Calculate functional Ecad level  $P_n$  (eq 1)*

*Calculate bonding probability  $BP_{mn}$  (eq 2)*

*Generate random number,  $k$*

*Form stable adhesion with all neighbours with  $BP_{mn} > k$*

*For every existing stable contact*

*Update contact length (eq 3)*

**2. Transient contact**

*If num\_curr\_bond < 6*

*Find separation to all neighbours within  $5\mu\text{m}$*

*For each non-bonded neighbour*

*Calculate length of transient contact (eq 4)*

This phenomenological relationship produces a range of contact lengths that give reasonable agreement with that observed in microscopy images of growing NHU cell cultures. At every iteration, each agent calculated the value of  $clen_{mn}$  for each of its transient contacts, and the sum of these values,  $tlen_m$ , was used in the migration rule (see equation 4).

2.5.2 Morphological Behaviour

Whilst cells maintain a spherical morphology in suspension, once plated on a 2D substrate, cultured cells have been observed to increase their surface area, assuming a more flattened morphology (e.g. Nelson and Chen, 2002). At high density, cells will become increasingly ‘squashed’ by their neighbours, and once again, reduce their surface area to compensate. This behavior is accounted for in the model by allowing cells to actively ‘spread’ to a maximum of 1.5 times their initial rounded radius in low density, and to round to their original radius in high density. The decision for an individual agent to spread or round is determined by the magnitude of the compressive force returned by the overlap elimination algorithm (see section 2.5.5). Cells

are permitted to spread only for compressive force values of less than 5 units, and will round for higher compression values. This rule is summarised in box 2.

**BOX 2 - Morphology Rule**

*If total compressive force  $< 5$  and  $xy$ -radius  $< 15 \mu\text{m}$*

*Increase  $xy$ \_radius by 10%*

*Reduce  $z$  radius to maintain a constant volume*

*Else if total compressive force  $\geq 5$*

*Decrease  $xy$ \_radius by 1%*

*Increase  $z$  radius to maintain a constant volume*

*2.5.3 Migratory Behaviour*

This rule is summarised in box 3. In our earlier agent models (Walker et al., 2004a; Walker et al., 2004b), only cells without intercellular contacts were able to migrate. Introduction of the modified bond probability rules and the concept of transient contacts described above, resulted in very limited migration, even in low calcium conditions. This situation did not mirror that observed in real NHU cell cultures (e.g. note the movement of cells C and D in figure 3, which continue migrating in spite of their interaction). Hence, new rules were introduced that determined the ability of an agent to migrate based on the difference between the active migration force and intercellular adhesion force resulting from stable and transient cell contacts.

The active migration force,  $MF$ , has been reported to be approximately 20 nN (Lee et al., 1994), and the adhesion force arising from normal E-cadherin mediated interactions between pairs of cells has been estimated to be approximately 100 nN after 30 minutes ( $AF1$ ), and 200 nN after one hour ( $AF2$ ) of intercellular contact (Chu et al., 2004). Published data also suggests that when E-cadherin amounts are varied, the adhesion force is linearly related to the square of the amount of E-cadherin present at the cell surface (Chu et al, 2004). In the case of transient contacts, surface tension per unit length ( $ST$ ) between non-adherent cells has been calculated to be approximately 0.32nN per micrometre of boundary in contact (Foty and Steinberg, 2005). Taken together, these observations lead to the following formulation for total adhesion force,  $AF$ , in nN, acting on the  $m$ th cell:

$$AF_m = (ST * tlen_m) + AF1 \sum_{n=1}^{N1} P_m P_n + AF2 \sum_{k=1}^{N2} P_m P_k \quad (4)$$

where  $tlen_m$  is the length of cell boundary in micrometres involved in transient contacts (the summation of  $clen_{mn}$  values calculated according to equation 3 above),  $N1$  and  $N2$  are the number of E-cadherin mediated interactions that have existed for less and more than one hour respectively, and  $P_m$  and  $P_n$ , or  $P_k$  are the amounts of functional E-cadherin expression by the two cells involved in these interactions (dimensionless).

The model rule implemented was that a total intercellular adhesion force of less than 20 nN would result in migration for a particular cell, but for larger values, the cell is not permitted to migrate. The maximum migration velocity,  $v_{max}$ , was estimated from time-lapse images of cultured NHU cells (in 0.09mM calcium) to be in the region of 80 $\mu$ m/hour. For cells with normal functional E-cadherin expression, this effectively means that cells with one or more E-cadherin contacts are prevented from migration (as was the case in the earlier versions of our model), but that cells with contacts defined as transient, or mediated by sub-normal E-cadherin, may be permitted to migrate.

### **BOX 3 - Migration Rule**

*If total compressive force < 5*

*Calculate surface tension force due to transient contacts*

*Calculate total adhesion force due to E-cadherin mediated contacts (eq 5)*

*If total intercellular force < migratory force*

*If random no. < 0.1*

*Randomly alter current direction by up to 90 degrees*

*Calculate new x co-ordinate*

*Calculate new y co-ordinate*

*Adjust position if crossed model edge*

#### *2.5.4 Cell cycle regulation and cell contact*

This rule is summarised in box 4. As described in Walker et al. (2004a), agents contain memory parameters representing their current position in a particular phase of the cell cycle. The G1 phase

includes a checkpoint at which cells must either commit to progressing through the rest of the cycle, ultimately resulting in a mitotic division, or enter the G0 (quiescent) phase. As in our previous model, contact inhibition of growth is represented by the rule that agents with four or more E-Cadherin mediated contacts arrest in G0. Ultimately, it is our intention to replace this phenomenological rule with a more sophisticated model of the mechanisms governing contact inhibition (see Discussion), but this simplistic representation was deemed sufficient for the simulations described here.

**BOX – 4 Cell Cycle rule**

*If cell is halfway through G1*  
     *if condition1=true & condition2=true & condition3=true*  
         *Increment cycle step and grow*  
     *else*  
         *Enter G0*  
*else if cell is elsewhere in G1*  
     *Increment cycle step and grow*  
*else if cell is at end of G1 phase*  
     *progress to S/G2 phase*  
*else if cell is in G0*  
     *if condition1=true & condition2=true & condition3=true*  
         *Re-enter G1, increment cycle step and grow*  
     *else*  
         *Remain in G0*  
*else if cell is in S/G2 phase*  
     *Increment cycle step*  
*else if cell is at end of S/G2 phase*  
     *Progress to M phase*  
*else if cell is in M phase*  
     *Increment cycle step*  
*else if cell is at end of M phase*  
     *Divide*

**Condition 1** (*juxtacrine condition*) – *cell has maintained at least one contact (stable or transient) for  $\geq 8$  hours*

**Condition 2** (*contact inhibition condition*) – *cell has  $\leq 4$  stable contacts*

**Condition 3** (*morphology condition*) - *cell has radius in xy plane  $\geq 15\mu\text{m}$*

The influence of cell shape on growth was also included, with cells allowed to progress only once they had assumed a flattened morphology on the substrate (based on experimental observations in Nelson and Chen (2002)). Cells that have reduced their substrate contact area in response to compressive forces in high density culture will eventually exit the mitotic cycle into G0. This rule remains unchanged for this study.

As we describe in Section I above, we have incorporated the requirement that cells must maintain at least one intercellular contact (stable or transient) to be released from G0 at the start of the simulation. The latter represents the concept of cell cycle modulation via juxtacrine signaling mechanisms explored in a recent study (Walker et al., 2008).

#### 2.5.5 Overlap elimination algorithm

Following each iteration, any overlap between agents (represented as circles in the plane of the substrate) due to movement, growth and division was resolved by application of a simple numerical algorithm which calculated displacement due to agent overlaps (interpreted as repulsive contact forces in arbitrary units) until equilibrium was reached, or specified convergence criteria were met. New position data, along with any residual overlap (interpreted as residual compressive force), was passed back to the agent model for the next time step, where, according to the morphology rule, it could result in cells reducing their radius in the plane of the substrate, and ultimately, exiting the cell cycle. It is important to note that this algorithm deals with “passive” shifting of the agents by relatively small distances in order to eliminate overlap only. “Active” movement mechanisms (e.g. migration, cell division) are handled entirely by the rule-based model.

The acceleration induced in the  $i$ th cell, by the force exerted by its  $n$  neighbours is given by Newton’s second law, with damping:

$$m_i \ddot{u}_i + c_i \dot{u}_i = \sum_{j=1}^n F \quad (5)$$

where  $m_i$  is the mass of the cell,  $c_i$  is its damping constant and  $u$  is its displacement. As the cells only interact in two dimensions, the ‘mass’ of the cell is based on the planar area of the cell, assuming a unit density:

$$m_i = \pi r_i^2 \quad (6)$$

The inclusion of this inertial term resulted in a tendency of smaller cells to be shifted more than larger cells when subject to intercellular forces.

The damping constant,  $c_i$  is proportional to the mass of the cell:

$$c_i = \alpha m_i \quad (7)$$

where the proportionality constant  $\alpha$  is assigned according to the global location of the cell. By default,  $\alpha=0.1$ , but cells close to the edge of the model are given higher damping factors to inhibit their movement and prevent them being pushed off the edge of the model. Damping factors in the  $x$  and  $y$  direction can be manipulated independently, thus a cell may be more easily pushed in one direction than the other.

All agent locations and radii are passed from the agent model to the physical model. For each ‘physical’ iteration, a check is made to identify with which nearby cells an agent is overlapping. In addition, a list of the flags of other agents to which it has formed an intercellular bond is passed, and an attractive force is assumed to exist between the latter in order to counteract any tendency for bonded cells to be forced apart. Forces are assumed to be zero between agents that are neither overlapping, nor bonded.

The repulsive force exerted the cell  $i$  by neighbour  $j$  is defined to be proportional to the overlap or edge separation  $O_{ij}$  between the cells.

$$F_{ij} = k_{ij} O_{ij} \quad (8)$$

where  $k_{ij}$  is an arbitrary ‘stiffness’ constant defined to be equal to the inverse of the separation of the centres of cells  $i$  and  $j$ . If cells  $i$  and  $j$  have radii  $r_i$  and  $r_j$  and are located at  $(x_i, y_i)$  and  $(x_j, y_j)$  respectively, then:

$$O_{ij} = \sqrt{(x_j - x_i)^2 + (y_j - y_i)^2} - (r_i + r_j) \quad (9)$$

Note that the signs of the constants are constructed in such a way that cells experience a repulsive force from overlapping neighbours, and an attractive force from bonded neighbours that may be separated by a small distance.

Assuming the vector  $i \rightarrow j$  is orientated at angle  $\theta$  with respect to the  $x$  axis, resolving into two orthogonal directions and substituting into (9) gives:

$$F_{ij(x)} = k_{ij} \left\{ (x_j - x_i) - (r_i + r_j) \cos \theta \right\} \quad (10a)$$

$$F_{ij(y)} = k_{ij} \left\{ (y_j - y_i) - (r_i + r_j) \sin \theta \right\} \quad (10b)$$

The co-ordinates of cell  $i$  at time  $t$  are the co-ordinates  $(x_{0i}, y_{0i})$  at the previous time step plus the displacement  $u_{xi}, u_{yi}$  during the current time step, so equation 10a can be written:

$$F_{ij(x)} = k_{1ij} \left\{ (x_{0i} - x_{0j}) + (u_{xi} - u_{xj}) \right\} - k_{2xij} (r_i + r_j) \quad (11a)$$

and likewise for equation 10b:

$$F_{ij(y)} = k_{1ij} \left\{ (y_{0i} - y_{0j}) + (u_{yi} - u_{yj}) \right\} - k_{2yij} (r_i + r_j) \quad (11b)$$

where  $k_1$  and  $k_{2x}$  are constants depending on the location of the two cells:

$$k_{1ij} = \frac{1}{\sqrt{(x_j - x_i)^2 + (y_j - y_i)^2}} \quad (12a)$$

$$k_{2xij} = \frac{\cos \theta}{\sqrt{(x_j - x_i)^2 + (y_j - y_i)^2}} \quad (12b)$$

$$k_{2,yij} = \frac{\sin \theta}{\sqrt{(x_j - x_i)^2 + (y_j - y_i)^2}} \quad (12c)$$

The value of the differential terms in equation 5 at time  $t$ , can be written as difference equations:

$$\ddot{u}_{i,t} = \frac{u_{i,t} - 2u_{i,t-\partial t} + u_{i,t-2\partial t}}{\partial t^2} \quad (13a)$$

$$\dot{u}_{i,t} = \frac{u_{i,t} - u_{i,t-\partial t}}{\partial t} \quad (13b)$$

where  $u_{i,t-\partial t}$  and  $u_{i,t-2\partial t}$  denote the displacement of the  $i$ th cell evaluated at the two previous time points. Substituting equations 11 and 13 a and b into 5 gives the complete equation of motion for cell  $i$  in the x direction:

$$m_i \left\{ \frac{u_{i,t} - 2u_{i,t-\partial t} + u_{i,t-2\partial t}}{\partial t^2} \right\} + \alpha_i m_i \left\{ \frac{u_{i,t} - u_{i,t-\partial t}}{\partial t} \right\} = \sum_{j=1}^n \left[ k_{1ij} \left\{ (x_{0i} - x_{0j}) + (u_{xi} - u_{xj}) \right\} - k_{2,xij} (r_i + r_j) \right] \quad (14a)$$

$$m_i \left\{ \frac{u_{i,t} - 2u_{i,t-\partial t} + u_{i,t-2\partial t}}{\partial t^2} \right\} + \alpha_i m_i \left\{ \frac{u_{i,t} - u_{i,t-\partial t}}{\partial t} \right\} = \sum_{j=1}^n \left[ k_{1ij} \left\{ (y_{0i} - y_{0j}) + (u_{yi} - u_{yj}) \right\} - k_{2,yij} (r_i + r_j) \right] \quad (14b)$$

Similar equations can be assembled to describe the x and y displacements of every cell in the model. Equation 14 a and b can then be rearranged:

$$\left[ \frac{\alpha M}{\partial t} + \frac{M}{\partial t^2} \right] u_{x,t} = \left[ \frac{2M}{\partial t^2} + \frac{\alpha M}{\partial t} \right] u_{x,t-1} - \left[ \frac{M}{\partial t^2} \right] u_{x,t-2} + \sum_{j=1}^n \left\{ k_{1ij} \left\{ (x_{0j} - x_{0i}) + (u_{xj,t-1} - u_{xi,t-1}) \right\} - k_{2,x} (r_i + r_j) \right\} \quad (15a)$$

$$\left[ \frac{\alpha M}{\partial t} + \frac{M}{\partial t^2} \right] u_{y,t} = \left[ \frac{2M}{\partial t^2} + \frac{\alpha M}{\partial t} \right] u_{y,t-1} - \left[ \frac{M}{\partial t^2} \right] u_{y,t-2} + \sum_{j=1}^n \left\{ k_{1ij} \left\{ (y_{0j} - y_{0i}) + (u_{yj,t-1} - u_{yi,t-1}) \right\} - k_{2,y} (r_i + r_j) \right\} \quad (15b)$$

The above can be solved explicitly to give  $u_{x,t}$  and  $u_{y,t}$  for every cell at every time step. The updated position will thus depend upon the displacements at the previous two time steps. This algorithm is run until empirically determined convergence criteria are fulfilled, or for a maximum of 200 iterations. The upper limit is required to allow for situations where the model approaches confluence and convergence will never be reached. In this case, any residual ‘force’ or overlap is passed back into the agent model, along with the updated cell locations. This is interpreted as compressive force, resulting in subsequent rounding of the cells according to the morphology rule (see section 2.5.2 above).

## 2.6 Sensitivity Testing

In order to ascertain whether the model predictions were dependent on particular parameter values, a sensitivity analysis was carried out on a selection of parameters associated with each of the agent rules sets. Priority was given to parameters that were estimated, rather than those extracted directly from the literature or from experimental data (e.g. observation of time-lapse images). Parameters subjected to sensitivity testing are indicated in table 2.

Each of a total of ten parameters was perturbed in turn by between 10 and 50% of the default value, and the results of the subsequent simulations analysed in order to assess the sensitivity. This analysis was restricted to 100% normal (EC-N) or 100% abnormal (EC-A) populations only, and three replicate simulations were carried out for each test using different randomly assigned distributions of seeded agents and varying random number generator seeds to account for variation due to stochastic effects.

A quantitative measure of sensitivity to each parameter was obtained by fitting a sigmoidal function to each mean growth curve, and comparing the parameters describing this function to those obtained from the unperturbed simulation. As shown in figure 4, the sigmoidal function describing total cell number,  $N$  at time  $t$  is given by:

$$N(t) = N_0 + \frac{a}{1 + \exp[c(t - b)]} \quad (16)$$

were  $N_0$  is the starting cell number (fixed at 200)  $a$  is the maximum cell number,  $c$  is the maximum gradient of the curve and  $b$  is the time point at which this maximum gradient occurs.

Curve fitting was carried out using Matlab's optimisation toolbox (Mathworks.com).

Parameter Name	Application	Value	Source	Sensitivity test?
<b>Adhesion rule</b>				
$q$	Equation 1 exponent	1/3	estimated	Y
$A, C, M, B, T$	Equation 2 parameters	A= 0.1, C= 0.57, M= 1mM, B= 1, T =1	(Baumgartner et al., 2000)	N
$p$	Equation 3 parameter controlling maximum length of transient contact	1.5	estimated	Y
$max\_sep$	Equation 3 parameter – maximum separation at which cells can form an initial contact	5 $\mu$ m	Estimated from time-lapse images	Y
<b>Migration/morphology rule</b>				
$CF$	Critical compressive force at which cells cease actively migrating and round up	5 (arbitrary units)	estimated	Y
<b>Migration rule</b>				
$MF$	Active migration force	20nN	(Lee et al., 1994)	N
$ST$	Eq. 4. Surface tension per unit length	0.32nN/ $\mu$ m	(Foty and Steinberg, 2005)	Y
$AF1$	Eq. 4. Adhesive force due to nascent (< 1 hour old) E-cadherin mediated contacts	100nN	(Chu et al., 2004)	Y
$AF2$	Eq. 4. Adhesive force due to > 1 hour old E-cadherin mediated contacts	200nN	(Chu et al., 2004)	Y
$v_{max}$	Maximum migration speed	80 $\mu$ m/hour	Estimated from time-lapse images	Y
<b>Cell cycle rule</b>				
$cyc\_len$	Cell cycle length (if no G0 entry)	15 hours	(Southgate et al., 1994)	N
$ci\_bond$	Number of bonds required for contact inhibition (G0 entry)	4	estimated	Y
$min\_contact\_time$	Minimum intercellular time required for S phase entry	4hours	estimated	Y
$min\_size$	Minimum radius in xy plane required for S phase entry	15 $\mu$ m	estimated	Y

**Table 2 Summary of parameters used in agent model**

Finally, in order to assess the sensitivity to edge effects, simulations for 100% normal and 100% abnormal populations were also carried out with the substrate size fixed at 2mm x 2mm and a seeded population of 800 agents.

### 3. RESULTS

#### 3.1 Simulation results

Figure 5 shows growth curves obtained for each of the simulations listed in Table 1. Error bars represent the standard deviation of three replicate simulations. Data are plotted only at intervals of 5 iterations for clarity.

In the case where all cells expressed normal amounts of E-cadherin (simulation 1 – figure 5a), population growth depended on the concentration of exogenous calcium. Initially, there was no growth in either low (0.09mM) or physiological (2.0mM) exogenous calcium due to the lag phase where cells take several hours to adhere to the substrate, then migrate to form initial intercellular contacts. As described above, once a cell maintained intercellular contacts for a period not less than 4 hours, it was permitted to re-enter the cell cycle, resulting in cell division approximately 10 hours later.

After approximately 15 hours, cells in 2.0mM calcium expanded in number more quickly (due to the increased tendency to maintain intercellular contact and hence greater propensity to fulfill the conditions to re-enter the cell cycle). The periodicity that can be seen in the growth curves at early time points reflects the synchronicity in cell cycle phase – all cells were initially in G0 and were released into the cell cycle within a relatively small number of iterations. Cell numbers in the low calcium environment initially increased more slowly, but as more cells were gradually produced by mitosis, contacts become more frequent, releasing yet more cells from G0 and the population began to expand exponentially. The total number of cells in the population maintained in the low calcium environment overtook that in physiological calcium after approximately 130 iterations (~2.7 days). As confluence was approached, the high number of stable, E-cadherin

mediated contacts resulted in many cells in physiological calcium becoming contacted-inhibited and re-entering G0. High cell density resulted in some cells in 0.09mM calcium also forming E-cadherin mediated contacts (this is supported experimentally by observations from immunofluorescence images of high density urothelial monolayers), but most cells in low calcium became quiescent due to increasing cell compression and the minimum radius rule (see box 4). At the end of the simulation period (representing approximately 4.7 days), the virtual population ‘cultured’ in 2 mM calcium conditions contained approximately 47% fewer cells relative to the equivalent low calcium simulations.

Inspection of figure 5 b-f) suggests that this pattern of normal population growth could be modified by a relatively small proportion of abnormal cells. Figure 5 b shows that when only 10% of the seeded population had inactive E-cadherin, the difference in the growth rates in the different calcium environments was reduced, resulting in a difference in cell number of approximately 28% at confluence. Most significantly, cells with aberrant E-cadherin failed to form multiple stable contacts, even in physiological calcium and hence did not tend to become contact-inhibited when approaching confluence, resulting in a prolonged exponential growth phase before ultimately arresting as a result of the minimum radius rule. This pattern became increasingly evident as the proportion of abnormal cells in the seeded population was increased. When 75% of the initial population had abnormal E-cadherin expression (figure 5e), the effect of contact inhibition at high cell density was reduced to such a degree that there was virtually no difference in the final population density between simulations in virtual 2.0mM and 0.09mM exogenous calcium. However, normal cells in the physiological calcium environment in mixed populations were able to form stable contacts at a frequency sufficient to produce elevated growth rates at earlier time points (up to 150 iterations). The similarity between the blue and green curves in figure 5 a-f) suggests that E-cadherin mutation had a minimal effect on population growth in a low calcium environment.

Figure 6 shows the growth data for heterogeneous population simulations in 2.0mM exogenous

calcium. In this case, population increase (as a multiple of the plated cell number) for each sub-population (EC-N or EC-A) is plotted separately at each time point. For comparison purposes, the results for 100% EC-N and 100% EC-A (simulations 1 and 6) are plotted on each set of axes. As well as demonstrating the relative ability of each sub-population to expand over time, this also reveals how the growth characteristics of each population is changed relative to the homogeneous case by the interactions with the other cell type.

As shown in figure 6 a), whereas normal cells in 2.0mM calcium increased their numbers by a factor of approximately 8 during the course of the simulation, the mutated cell population expanded by approximately a factor of 18 in the same time period (note that the relatively large error bars for this curve relate to the small size of the absolute number of EC-A cells at  $t=0$  in this simulation). This was in spite of the fact that mutated cells had a slightly reduced growth advantage compared to EC-N cells when the culture was relatively sparse (before 110 iterations), due to their decreased tendency to form stable contacts. As the seeded fraction of abnormal cells was increased, their overall growth advantage relative to the EC-N population was gradually diminished and that of the latter increased. At starting ratios of 1:1 or above (figure 6 c and d), abnormal cells were actually at a slight disadvantage compared to normal cells due to their reduced likelihood of maintaining intercellular contact for a minimum of four hours (see section 2.5.4 and box 4), resulting in an initial delay in this sub-population re-entering the cell cycle.

Comparing the ability of sub-populations to expand in heterogeneous, relative to homogeneous cultures also revealed interesting results. When just 10% of the seeded population comprised EC-A cells, the steady state population of normal cells increased to 8 times the starting population over the simulation period (figure 6a), whereas this value for a purely homogeneous EC-N population was 6.5. This represents a 20% increase in the expansion of these cells. As the seeded fraction of EC-A cells was increased, the expansion of EC-N cells increased further (figure 6 b-d). This relates to a reduced effect from contact inhibition due to the inability of neighbouring EC-A cells to form stable contacts. The effect of EC-N cells on the expansion capacity of the EC-

A population is a little more complex. In situations where abnormal cells are present as a relatively small proportion of the seeded population, there was an early enhancement of growth amongst this sub-population due to the greater opportunity for intercellular contact (as abnormal cells may be 'trapped' by the colonies formed by their normal counterparts). However, as the growth of the normal population slowed upon approaching confluence due to contact inhibition, the abnormal cells continue to expand rapidly, leading to a relatively large increase in this sub-population. As the mix ratio became more balanced, and normal cells benefitted from the relative lack of contact inhibition, the opportunity for continued expansion of the mutated population was diminished. Finally, when abnormal cells are in the majority at the time of seeding, the opportunity for population expansion is actually reduced compare to a 100% abnormal population, due to competition for space with the rapidly expanding normal cells.

Figure 7 shows snapshots of the cell populations at iteration numbers 20, 50, 75 and 100 for homogeneous simulations 1 (both 0.09mM and 2.0mM calcium) and 6 (2.0mM calcium only). Figure 8 shows snapshots at the same time points for heterogeneous simulations 2-5. Movies corresponding to the simulations 1, 4 and 6 in both low and physiological calcium are provided as additional files 1-6. Inspection of figure 7 row *a* demonstrates that, as previously reported (Walker et al.,2004a), normal cells in 0.09mM calcium did not tend to grow in colonies but remain dispersed. In additional movie file 1, generated from the consecutive sequence of these snapshots, it can be seen that a large number of cells were migratory. Row *b* shows that normal cells in physiological calcium tended to grow in colonies and the corresponding movie (additional file 2) shows little individual cell migration. When all cells were mutated (figure 7 row *c* and additional file 6), there was some grouping of cells, but the cellular distribution was dispersed and similar in appearance to the low calcium case (row *a*).

When mutated cells were present as sub-populations (figure 8), they tended to be pushed to the outside of the colonies, and movies show frequent migration of these cells between colony edges (e.g. see additional file 4). In the case where the mutated population was dominant (row *d*),

colony formation amongst the remaining normal subpopulation was significantly disrupted. As the mixed population simulations reached confluence, abnormal cells formed islands surrounded by normal cells and, due to the lack of contact inhibition, these islands continued to expand significantly after confluence was reached (as for EC-N cells in low calcium, these cells eventually entered G0 due to the rules that state that cells become increasingly rounded in response to intercellular compression forces, and become quiescent when their radius in the plane of the substrate falls below a threshold value). Inspection of movies corresponding to low calcium simulations showed little difference in behaviour according to the proportion of EC-A cells (e.g. compare additional files 1, 3 and 5).

By examining the behaviour of individual subsets of cells in the model in more detail, it was possible to ascertain whether the alterations observed in the population level dynamics were a result of the altered phenotype of the abnormal cells only, or whether the presence of these cells could also modify the behavior of their normal counterparts. Figure 9a and c show the mean number of stable contacts per cell in the homogeneous and heterogeneous 2.0mM calcium simulations for EC-N and EC-A cells respectively. Figure 9b and d shows the fraction each subpopulation that actively migrated at each iteration. This figure demonstrates that, as expected, the mean number of stable contacts established by EC-A cells is consistently lower than those established by EC-N cells, irrespective of total cell density. Consequently, the migration rate for EC-A cells is consistently higher than for normal cells.

It can be seen that the presence of 10% mutated cells slightly reduces the mean number of stable contacts maintained by normal cells. This effect is enhanced as the seeded fraction of mutated cells is increased and the normal cells in these simulations adopt a more migratory phenotype. This suggests that the influence of the mutated cells on the mixed population dynamics is complex and cannot simply be attributed directly to an altered cell proliferation rate amongst the mutated sub-population.

### 3.2 Results of Sensitivity Testing

The parameters selected for sensitivity testing are listed in Table 2. As described in section 2.6, a sigmoidal curve was fitted to the mean growth curve obtained for each of the parameter perturbations. Parameter values obtained for each test were then assessed against those obtained for the control simulations (no parameter perturbation) in order to give a quantitative measure of sensitivity,  $S$ :

$$S_n = \frac{\Delta output}{\Delta input} = \frac{(P_n - P_0) / P_0}{(I_n - I_0) / I_0} \quad (17)$$

where  $S_n$  is the sensitivity to parameter  $n$ ,  $P_n$  is the output ( $a$  or  $b$  in equation 16) for the perturbed simulation,  $P_0$  is the equivalent parameter for the control simulations,  $I_n$  is the value of the input parameter for the test simulation and  $I_0$  is the equivalent value from the control simulations (given in Table 2).

This process was carried out for the parameters  $a$  and  $b$  in equation 16. These relate to directly observable characteristics of the growth curve ( $a$  is equivalent to the steady state population number and  $b$  to the time point of maximum population growth, both of which have been shown to vary according to exogenous calcium concentration). The parameter  $c$ , which relates to the maximum curve gradient, was not observed to vary significantly, and results are not presented. Both a quantitative and a qualitative analysis of sensitivity data was carried out.

Figure 10 shows the sensitivity factors calculated based on the values of  $a$  and  $b$  above plotted on a 3D surface plot. The x and y axis represent the sensitivity factors for  $a$  and  $b$  respectively (as calculated according to equation 17) for any parameter with a  $S_n$  value greater than 0.1. The z axis (surface height) is used for illustrative purposes only to emphasise the relative sensitivity factors. Separate plots are used to represent 100% EC-N cells in low calcium (figure 10a), 100% EC-N cells in physiological calcium (figure 10b) and 100% EC-A cells in low calcium (figure 10c - results did not depend on exogenous calcium in this case). Plots d-f are rescaled versions of a-c to

more clearly display the clusters of parameters with sensitivity factors  $<1$ .

A qualitative analysis was also carried out where  $S_n$  values were ranked as low ( $<0.5$ ), intermediate ( $0.5-1.0$ ) or high ( $>1.0$ ) for each simulation category and each parameter in turn was checked in order to ascertain whether variation within the tested limits resulted in the violation of the four primary growth characteristics reported above:

- I. Populations of normal cells enter the exponential phase more rapidly in physiological calcium compared to low calcium
- II. Populations of normal cells in low calcium reach a higher steady state density than those cultured in physiological calcium.
- III. Populations of mutated cells grown in either calcium concentration reach a steady state population number which is approximately equivalent to normal cells grown in physiological calcium
- IV. Populations of mutated cells grown in either calcium concentration enter the exponential phase at approximately the same interval as normal cells cultured in low calcium.

The results of the qualitative sensitivity analysis are shown in Table 3.

As shown in figure 10 and table 3, certain parameters do have high sensitivity values in terms of their influence on both final population density ( $a$ ) and time to reach maximum growth rate post-seeding ( $b$ ). Specifically, these are the parameter  $ci\_bond$ , which dictates the maximum number of E-cadherin mediated contacts required for contact inhibition (this is critical in determining the final cell number in normal physiological calcium simulations), and  $min\_size$ , which determines the minimum x-y plane radius at which cells are permitted to proceed through the cell cycle checkpoint (important in determining the steady state population in all simulations). Parameters with a moderate influence on observed population growth include  $vmax$  (maximum migration velocity), and the minimum time a contact must be maintained to allow cell cycle progression. However, whilst these parameters may influence the *absolute* values associated with

population growth, it was observed that none of the sensitivity tests resulted in a violation of the *general relative characteristics* of growth reported for either the 100% normal, or 100% mutated cell populations.

Finally, the growth characteristics of 100% normal, or 100% mutated cell populations were found to hold for simulations carried out on a 2mm x 2mm virtual substrate, which suggests that our results are not sensitive to boundary effects (results not shown).

Parameter Name	Maximum Sensitivity Factor			Observation violated			
	100% EC-N, [Ca <sup>2+</sup> ]= 0.09mn	100% EC-N, [Ca <sup>2+</sup> ]= 2.0mM	100% EC-M, [Ca <sup>2+</sup> ]= 0.09mn	I	II	III	IV
<b>Adhesion rule</b>							
<i>Q</i>	L	L	L	x	x	x	x
<i>P</i>	L	L	L	x	x	x	x
<i>max sep</i>	L	L	L	x	x	x	x
<b>Migration/morphology rule</b>							
<i>CF</i>	L	L	L	x	x	x	x
<b>Migration rule</b>							
<i>ST</i>	L	L	L	x	x	x	x
<i>AF</i>	L	L	L	x	x	x	x
<i>v<sub>max</sub></i>	M	M	M	x	x	x	x
<b>Cell cycle rule</b>							
<i>ci bond</i>	M	H	L	x	x	x	x
<i>min contact time</i>	H	M	M	x	x	x	x
<i>Min size</i>	H	H	H	x	x	x	x

**Table 3** Qualitative results of sensitivity analysis. Maximum sensitivity factors associated with each model parameter are classified as low (L) - <0.5, medium (M) 0.5-1.0 or high (H) - >1.0. An x indicates that the relevant growth characteristic is not violated (see text in Section 3.2 for further details).

#### 4. DISCUSSION

Understanding the mechanisms by which cell-cell interactions determine cellular behavior is central to understanding not only normal tissue growth but also neoplastic development. We have described the extension and application of an agent-based model of epithelial cells in culture in order to explore these concepts. In particular, we have focused on the adhesion protein E-cadherin, its role in governing cell:cell adhesion and modulating proliferation under different environmental conditions and the consequences of loss of function from all, or a subset of cells.

We have included an enhanced rule set describing adhesion, migration and proliferation effects in response to current and recent cell-cell contacts. This rule set is based on our own observations of the behaviour of NHU cells in culture (as revealed by time-lapse microscopy), data reported in the biological literature, and our own previously developed multi-scale computational exploration of juxtacrine intercellular signaling mechanisms (Walker et al., 2008). In this previous paper, we described a potential pro-proliferative effect mediated by juxtacrine activation of EGFR that required direct contact with ligands on juxtaposed cell membranes, with frequent transient contacts or expanding E-cadherin bonded contacts required to maintain Erk in an active form over a period of several hours, as required to promote cell cycle progression (Roovers and Assoian 2000; Yamamoto et al., 2006). This informed a new rule, which can be considered an abstraction of this mechanism, stating that in order to progress through the G1/G0 checkpoint, a cell must have maintained intercellular contact for a continuous period of at least 4 hours.

Although the parameters defining this rule set (and in particular, the time period over which contact must be maintained) are essentially arbitrary, a good qualitative match with the growth of NHU cells cultured in low and physiological calcium conditions was obtained (figure 1 and figure 5a). A sensitivity analysis revealed that changes of  $\pm 2$  hours in this time threshold caused some change in the predicted growth rates, but the relative patterns of growth in the two environments were not significantly affected. Thus, our rule set was deemed to be suitably robust for the computational exploration described here. It should be noted that we have ignored the effect of soluble growth factors, which might be expected to have a similar growth enhancing effect on cells in both low and physiological calcium environments.

We have applied our model to investigate the behavior of mixed populations consisting of two sub-groups of cells: those that normally express E-cadherin and those in which this protein has been compromised or down regulated. Introduction of a sub-population of mutated or “anti-social” cells into the model yielded interesting predictions. The presence of even a relatively small fraction of mutated cells was predicted to affect the population growth characteristics, but

the degree to which population growth was modified was highly dependent on the extracellular environment of the cells. When the exogenous calcium concentration was very low, no significant effect was seen. These predictions highlight the importance of the role of the tissue environment in determining cellular behavior, reinforcing the concept that a particular genotype does not necessarily always yield the expected phenotype.

Varying the relative proportion of normal and abnormal cells in a physiological calcium environment suggested that the different cell sub-populations had a relative growth advantage or disadvantage that depended both on the mix ratio and the degree of confluence of the culture. In particular, our model predicted that even a small number of “anti-social” cells could modulate the confluent cell population density, as the lack of contact inhibition yielded a growth advantage in the mutated population as confluence was approached. As the fraction of the mutated population in the seeded culture was increased further, intercellular contact was disrupted to such a degree that proliferation in the sparse culture was negatively modulated, leading to an initial reduction in population growth rate. Under these conditions, cells with E-cadherin mutations were actually at a disadvantage, compared to those that could form stable contacts.

Previous publications (e.g Glazier and Graner, (1993); Hogeweg, (2000)) describe the computational exploration of the Differential Adhesion Hypothesis (reviewed in Foty and Steinberg, (2005)): the idea that differences in the adhesive properties of cells can drive tissue formation and embryogenesis, resulting in diverse tissue morphologies. Our simple rule-based model, coupled with a mathematical representation of rigid body interactions is in agreement with these more complex models, predicting an emergent behaviour whereby subpopulations of mutated cells were pushed to the outside of the colonies, or in the case where this population is dominant, disrupted colony formation amongst the remaining normal population.

Our model also predicted that population dynamics were not only *directly* influenced by the presence of abnormal cells in terms of a density-dependent growth advantage or disadvantage in relation to their normal untransformed counterparts, but also that the presence of these cells may

actually modify the behaviour of their normal neighbours. This results in an *indirect* modulation of population growth. As shown in Figure 6, the relative expansion capacity (cell number at steady state compared to seeded cell number) of normal cells in heterogeneous cultures, as compared to the homogeneous case, was progressively increased as the fraction of abnormal cells in the seeded population was increased, due to the reduced effect from contact inhibition at high density. This may have implications for the development of hyperplastic epithelium, where genetically ‘normal’ cells may proliferate excessively, potentially due to loss of contact inhibition cues in their local environment. Our results suggest that the appearance of even a relatively small number of cells whose ability to form stable contacts is genetically compromised could potentially provide such a cue for abnormal proliferative behaviour among their non-transformed counterparts.

As shown in figure 9a), the mean number of stable contacts among normal cells in mixed populations was decreased and their propensity to migrate increased, relative to cells in entirely normal populations, again, simply due to their interaction with abnormal cells which were less likely to form stable contacts. This ability of transformed cells to influence the behavior of normal cells is likely to be further modified in real biological tissue, for instance, through alterations in the production of excreted or surface bound growth factors which are not explicitly included in this model. This phenomenon may have important implications for understanding the process of neoplastic transformation and natural selection advantage.

In our simulations, we have assumed that the only change associated with the abnormal cells is their inability to form stable intercellular contacts. The requirement for sustained intercellular contact (comprising either stable, or serial transient contacts) to facilitate initial release from G1 still holds for our EC-A population. However, in many malignant cell types, there are multiple changes to cell phenotype, particularly involving growth control mechanisms, which have not been considered here.

In this study, we have modelled cell populations that are well mixed and initially at low density.

During *in vivo* malignant transformation, tissues are confluent, and tumours may arise and grow in spatially-confined locations. Modelling the behaviour of a single, or small group of transformed cells in a confluent, quiescent monolayer would allow us to explore the concept that mutated cells may remain nascent within a normal tissue until an event, such as tissue injury, acts to drive tumour formation as part of a proliferative wound healing response.

Recently, Ramis-Conde et al., (2008;2009) used a multiscale model of E-cadherin/ $\beta$ -catenin signaling in confluent cell populations to demonstrate that the loss of adhesion in a small area could give rise to a 'wave' of cell detachment propagating from the initial site of disruption. The mechanism they postulated was that  $\beta$ -catenin released from intercellular contacts acts as a transcription factor to upregulate expression of genes responsible for promoting migratory behaviour, ultimately resulting in an epithelial-mesenchymal transition. The potential role of cell proliferation or interaction(s) with the extracellular environment was not explicitly explored in their model. However, these computational studies can potentially play an important role in probing the relative importance of cellular level phenomena in determining tissue characteristics.

It is unavoidable that some parameters in any computational or mathematical model must be either estimated or assumed, as exact values are difficult or impossible to obtain experimentally. The process of methodological sensitivity testing of model parameters is important in identifying particular control parameters that are critical in regulating model behaviour. Our sensitivity analysis revealed that parameters associated with cell cycle control were most important in determining *quantitative* aspects of population growth, though none of our parameter perturbations violated the relative growth characteristics under different simulation conditions and hence, our model can be assumed to be *qualitatively* robust. Parameters controlling migratory and adhesive behaviour (which were generally taken directly from the literature, or derived from observation of time-lapse images) generally had a much smaller influence on the model.

In an agent-based model, certain parameters may themselves represent abstractions of particular

underlying biological mechanisms. An example of the latter is the rule in our model, which states that a cell with four or more stable intercellular contacts becomes contact-inhibited and enters the G0 phase. This simplistic rule is intended to represent intracellular processes relating to cell contact and control of proliferation, some of which are yet to be fully elucidated. A candidate mechanism for contact-mediated downregulation of proliferation is the sequestration of the intracellular protein  $\beta$ -catenin to intercellular contacts, thus preventing it from entering the nucleus where it can act as a transcription factor in cell cycle progression (Stockinger et al., 2001). We are currently in the process of developing a more detailed mechanistic model of this process, which will ultimately replace our simple contact inhibition rule, and hence eliminate the *ci\_bond* parameter which has a relatively strong influence on steady-state population in physiological calcium concentrations. This ability to extend model complexity as deemed necessary by sensitivity analysis, or comparison with experimental data is an inherent advantage of the agent-based paradigm. Other important parameters, including *min\_contact\_time* and *min\_size* may in future be more tightly constrained by further analyses of time-lapse microscopy data.

Although particular model parameters (e.g. minimum cell cycle duration, migration speed) are set to reflect the behavior of a particular cell type (human urothelial cells), many of the behaviors represented by the model (proliferation, adhesion, migration) are generic across many biological tissue types. Application of our model to other tissue types would simply involve adjusting the appropriate parameters. The addition of new rule sets in order to represent different biological processes (e.g. differentiation, stratification) is also a relatively trivial task.

As discussed above, some parameters in our model are currently, by necessity, arbitrary. However, the ability of the model to predict experimentally observed emergent behaviour is a good indication of its robustness. In order to test this, we intend to carry out *in vitro* experiments on mixed populations of human urothelial cells, where E-cadherin expression in a subset of cells has been altered by genetic manipulation. Comparison of our model predictions with

experimentally-acquired growth curves and also observation of individual cell behaviour by time-lapse microscopy will either support our current model rule set, or direct further *in vitro* and computational experimentation. This iterative, symbiotic relationship between *in vitro* and *in vitro* experimentation is essential for enhancing our understanding of biological behaviour and will ultimately result in validated rule sets that can be translated into three dimensional geometries that are more representative of *in vivo* tissue environments.

## 5. CONCLUSION

We have described simulations generated by our agent-based model of growing cell populations consisting of sub-groups of cells expressing normal and abnormally low amounts of the adhesion molecule E-cadherin. Our model has predicted that sub-populations of abnormal cells can influence population growth dynamics, both directly, and via their interactions with normal, E-cadherin intact cells. The magnitude of the effect of E-cadherin loss-of-function amongst a subpopulation of cells on the overall population dynamics is not pre-determined, but also depends on the extracellular calcium concentration.

Our study demonstrates that individual- or agent-based modeling of mixed cell populations can provide an insight into biological processes that may be non-intuitive. Ultimately, it is anticipated that understanding complex cellular interactions will enhance our knowledge and understanding of the development of neoplasia in epithelial tissues and provide new insight into the design of treatment regimens.

### **Authors' contributions**

DW developed the models, carried out simulations, analysed the model results and drafted the manuscript. NTG planned and carried out the time-lapse microscopy and cell count experimental studies and analysed the results. JS participated in the design and coordination of the

experimental study and helped to draft the manuscript. All authors jointly conceived the study and have read and approved the final manuscript.

### **Acknowledgements**

The authors would like to thank RCUK, who provide the Academic Fellowship held by DW. NTG carried out experimental work as a postdoctoral research fellow funded by the Engineering and Physical Sciences Research Council (EPSRC) on grant GR/S62338/01. JS holds a research chair supported by York Against Cancer. The authors would also like to acknowledge Professor Rod Smallwood, University of Sheffield, for coining the phrase ‘anti-social cells’.

### **REFERENCES**

- Adams, C. L., Chen, Y. T., Smith, S. J. and Nelson, W. J. (1998). Mechanisms of Epithelial Cell-Cell Adhesion and Cell Compaction Revealed by High-resolution Tracking of E-Cadherin-Green Fluorescent Protein. *J Cell Biol* **142**(4): 1105-1119.
- Anderson, A. R. and Chaplain, M. A. (1998). Continuous and discrete mathematical models of tumor-induced angiogenesis. *Bull Math Biol* **60**(5): 857-99.
- Baumgartner, W., Hinterdorfer, P., Ness, W., Raab, A., Vestweber, D., Schindler, H. and Drenckhahn, D. (2000). Cadherin interaction probed by atomic force microscopy. *Proc Nat Acad Sci USA* **97**(8): 4005-4010.
- Bentley K, Gerhardt H and Bates PA (2007). Agent-based simulation of notch-mediated tip cell selection in angiogenic sprout initialisation. *J Theor Biol* **250**(1): 25-36.
- Chu, Y.-S., Thomas, W. A., Eder, O., Pincet, F., Perez, E., Thiery, J. P. and Dufour, S. (2004). Force measurements in E-cadherin-mediated cell doublets reveal rapid adhesion strengthened by actin cytoskeleton remodeling through Rac and Cdc42. *J Cell Biol* **167**(6): 1183-1194.

- Conacci-Sorrell, M., Zhurinsky, J. and Ben-Ze'ev, A. (2002). The cadherin-catenin adhesion system in signaling and cancer. *J Clin Invest* **109**(8): 987-91.
- Drasdo D and Hoeme S (2005). A single-cell-based model of tumor growth: in vitro monolayers and spheroids. *Physical Biology* **2**(3): 133.
- Folcik, V. A., An, G. C. and Orosz, C. G. (2007). The Basic Immune Simulator: an agent-based model to study the interactions between innate and adaptive immunity. *Theor Biol Med Model* **4**: 39.
- Foty RA and Steinberg MS (2005). The differential adhesion hypothesis: a direct evaluation. *Developmental Biology* **278**(1): 255-263.
- Foty, R. A. and Steinberg, M. S. (1997). Measurement of tumor cell cohesion and suppression of invasion by E- or P-cadherin. *Cancer Res* **57**(22): 5033-6.
- Foty, R. A. and Steinberg, M. S. (2004). Cadherin-mediated cell-cell adhesion and tissue segregation in relation to malignancy. *Int J Dev Biol* **48**(5-6): 397-409.
- Glazier J A, Graner. F. (1993). Simulation of the Differential Adhesion driven Rearrangement of Biological Cells. *Physical Review E* **47**(3): 2128-2153.
- Grimm, V., Berger, U., Bastiansen, F., Eliassen, S., Ginot, V., Giske, J., Goss-Custard, J., Grand, T., Heinz, S. K., Huse, G., Huth, A., Jepsen, J. U., Jorgensen, C., Mooij, W. M., Muller, B., Pe'er, G., Piou, C., Railsback, S. F., Robbins, A. M., Robbins, M. M., Rossmannith, E., Ruger, N., Strand, E., Souissi, S., Stillman, R. A., Vabo, R., Visser, U. and DeAngelis, D. L. (2006). A standard protocol for describing individual-based and agent-based models. *Ecological Modelling* **198**(1-2): 115-126.
- Hogeweg, P. (2000). Evolving Mechanisms of Morphogenesis: on the Interplay between Differential Adhesion and Cell Differentiation. *Journal of Theoretical Biology* **203**: 317-333.
- Lee J, Leonard M, Oliver T, Ishihara A and Jacobson K (1994). Traction forces generated by locomoting keratocytes. *Journal of Cell Biology* **127**: 1957-1964.

- Liu, W., Nelson, C., Pirone, M. and Chen, C. (2006). E-cadherin engagement stimulates proliferation via Rac1. *J Cell Biol* **173**(3): 431-441.
- Mansury, Y., Kimura, M., Lobo, J. and Deisboeck, T. S. (2002). Emerging patterns in tumor systems: simulating the dynamics of multicellular clusters with an agent-based spatial agglomeration model. *J Theor Biol* **219**(3): 343-70.
- Nelson, C. M. and Chen, C. S. (2002). Cell-cell signalling by direct contact increases cell proliferation via a P13K-dependent signal. *FEBS Letters* **514**: 238-242.
- Pece S, Chiariello M, Murga C and Gutkind JS (1999). Activation of the protein kinase Akt/PKB by the formation of E-cadherin-mediated cell-cell junctions. Evidence for the association of phosphatidylinositol 3-kinase with the E-cadherin adhesion complex. *Journal of Biological Chemistry* **274**(27): 19347-19351.
- Pece S, Gutkind. J. S. (2000). Signaling from E-Cadherins to the MAPK pathway by the recruitment and activation of the epidermal growth factor receptors upon cell-cell contact formation. *Journal of Biological Chemistry* **275**(52): 41227-41233.
- Ramis-Conde, I., Drasdo, D., Anderson, A. R. and Chaplain, M. A. (2008). Modeling the influence of the E-cadherin-beta-catenin pathway in cancer cell invasion: a multiscale approach. *Biophys J* **95**(1): 155-65.
- Ramis-Conde, I., Chaplain, M. A., Anderson, A. R. and Drasdo, D. (2009). Multi-scale modelling of cancer cell intravasation: the role of cadherins in metastasis. *Phys Biol* **6**(1): 16008.
- Roovers, K. and Assoian, R. K. (2000). Integrating the MAP kinase signal into the G1 phase cell cycle machinery. *BioEssays* **22**: 818-826.
- Southgate, J., Hutton, K. R., Thomas, D. F. M. and Trejdosiewicz, L. K. (1994). Normal human urothelial cells in vitro: proliferation and induction of stratification. *Laboratory Investigation* **71**(4): 583-594.

- St Croix, B., Sheehan, C., Rak, J. W., Florenes, V. A., Slingerland, J. M. and Kerbel, R. S. (1998). E-Cadherin-dependent growth suppression is mediated by the cyclin-dependent kinase inhibitor p27 KIP1. *J Cell Biol* **142**(2): 557-571.
- Steinberg, M. L., Hwang, B. J., Tang, L. and Shah, M. A. (2008). E-cadherin gene alterations in gastric cancers in different ethnic populations. *Ethn Dis* **18**(2 Suppl 2): S2-70-4.
- Stockinger, A., Eger, A., Wolf, J., Beug, H. and Foisner, R. (2001). E-cadherin regulates cell growth by modulating proliferation-dependent beta-catenin transcriptional activity. *J Cell Biol* **154**(6): 1185-96.
- Takahashi, K. and Suzuki, K. (1996). Density-dependent inhibition of growth involves prevention of EGF receptor activation by E-Cadherin mediated cell-cell adhesion. *Exp Cell Res* **226**: 214-222.
- Tang, J., Ley, K. F. and Hunt, C. A. (2007). Dynamics of in silico leukocyte rolling, activation, and adhesion. *BMC Syst Biol* **1**: 14.
- Walker, D., Hill, G., Wood, S., Smallwood, R. and Southgate, J. (2004b). Agent-based computational modeling of wounded epithelial cell monolayers. *IEEE Trans Nanobioscience* **3**(3): 153-163.
- Walker, D., Southgate, J., Hill G, Holcombe, M., Hose, D., Wood, S., Macneil, S. and Smallwood, R. (2004a). The Epitheliome: modelling the social behaviour of cells. *Biosystems* **76**(1-3): 89-100.
- Walker, D. C., Georgopoulos, N. and Southgate, J. (2008). From pathway to population – a multiscale model of juxtacrine EGFR-MAPK signalling. *BMC Systems Biology* **2**(102).
- Yamamoto, T., Ebisuya, M., Ashida, F., Okamoto, K., Yonehara, S. and Nishida, E. (2006). Continuous ERK activation downregulates antiproliferative genes throughout G1 phase to allow cell-cycle progression. *Current Biology* **16**(12): 1171-1182.

## Figure Captions

Figure 1 Typical growth curves obtained from normal human urothelial (NHU) cells, cultured in low and physiological calcium ion concentrations

Figure 2 (a) Schematic showing simulation process (b) Information passed between agent model and 'physical' solver (a numerical algorithm which eliminates or minimizes cell overlap – see Walker et al, (2004a) for further details).

Figure 3 Time-lapse microscopy images of NHU cells cultured in 0.09mM (low) calcium. Frames taken at (a) 0 minutes, (b) 10 minutes and (c) 20 minutes, illustrating the persistence of large intercellular contacts between cell pairs A and B and C and D.

Figure 4 – Parameters derived from sigmoidal curve fit to modelled population growth characteristics. Parameter a represents to total cell number at steady state, and b to the time delay in reaching maximum growth rate.

Figure 5 Growth curves (total cell number against model iteration) obtained from mixed population simulations resulting from seeded populations consisting of (a) 100% EC-N, (b) 90% EC-N, (c) 75% EC-N, (d) 50% EC-N, (e) 25% EC-N and (f) 0% EC-N. Curves in (a) are repeated on all axes for comparison. Error bars indicate the standard deviation obtained from 3 separate simulations, and are plotted only every five iterations for clarity.

Figure 6 Fractional growth (total sub-population number at iteration divided by seeded sub-population number) for heterogeneous populations of normal and abnormal cells in 2.0mM (physiological) calcium (a) 90% EC-N (b) 75% EC-N (c) 50% EC-N (d) 25% EC-N. Growth curves

for homogeneous EC-N and EC-A cells (i.e. from simulations 1 and 6) are included on each set of axes for comparison.

Figure 7 Snapshots of normal (blue/dark) and E-cadherin mutant (green/light) cells at various time points during homogeneous simulations. Small spherical pink cells are mitotic (both normal and abnormal). Row a) Simulation1, 0.09mM exogenous calcium, b) simulation 1, 2.0mM calcium, c) simulation 6, 2.0mM calcium.

Figure 8 Snapshots of normal (blue/dark) and E-cadherin mutant (green/light) cells at various time points during heterogenous simulations in 2.0mM calcium. Small spherical pink cells are mitotic (both normal and abnormal).a) simulation 2, b) Simulation 3, c) simulation 4, d) simulation 5

Figure 9 (a) mean number of stable (E-cadherin-mediated) contacts per normal cell and (b) fraction of normal cells migrating (c) mean number of stable (E-cadherin-mediated) contacts per abnormal cell and (d) fraction of abnormal cells migrating in a physiological calcium (2.0mM) environment according to initial population mix ratio.

Figure 10 Results of sensitivity analysis presented as surface plots. x axis represents sensitivity of parameter  $a$ , y axis sensitivity to parameter  $b$  (see text and equations 16 and 17 for details), surface height and shading is for illustrative purposes only for a) 100% EC-N population in 0.09mM calcium, b) 100% EC-N population in 2.0mM calcium and c) 100% EC-A population in 2.0mM calcium. Plots d)-f) are zoomed in versions of a)-c) respectively, to highlight the effect of input parameters with sensitivity values  $< 1$ .

**Additional files****Additional file 1**

Virtual time-lapse movie of agent simulation of 100% EC-N cells in a low calcium (0.09mM) environment. Blue = EC-N cells, pink = cells in M phase of cell cycle. 1 frame = 30 minutes.

**Additional file 2**

Virtual time-lapse movie of agent simulation of 100% EC-N cells in a physiological calcium (2.0mM) environment. Blue = EC-N cells, pink = cells in M phase of cell cycle. 1 frame = 30 minutes.

**Additional file 3**

Virtual time-lapse movie of agent simulation of 50% EC-N cells and 50% EC-A cells in a low calcium (0.09mM) environment. Blue = EC-N cells, green= EC-A cells, pink = EC-N and EC-A cells in M phase of cell cycle. 1 frame = 30 minutes.

**Additional file 4**

Virtual time-lapse movie of agent simulation of 50% EC-N cells and 50% EC-A cells in a physiological calcium (2.0mM) environment. Blue = EC-N cells, green= EC-A cells, pink = cells in M phase of cell cycle. 1 frame = 30 minutes.

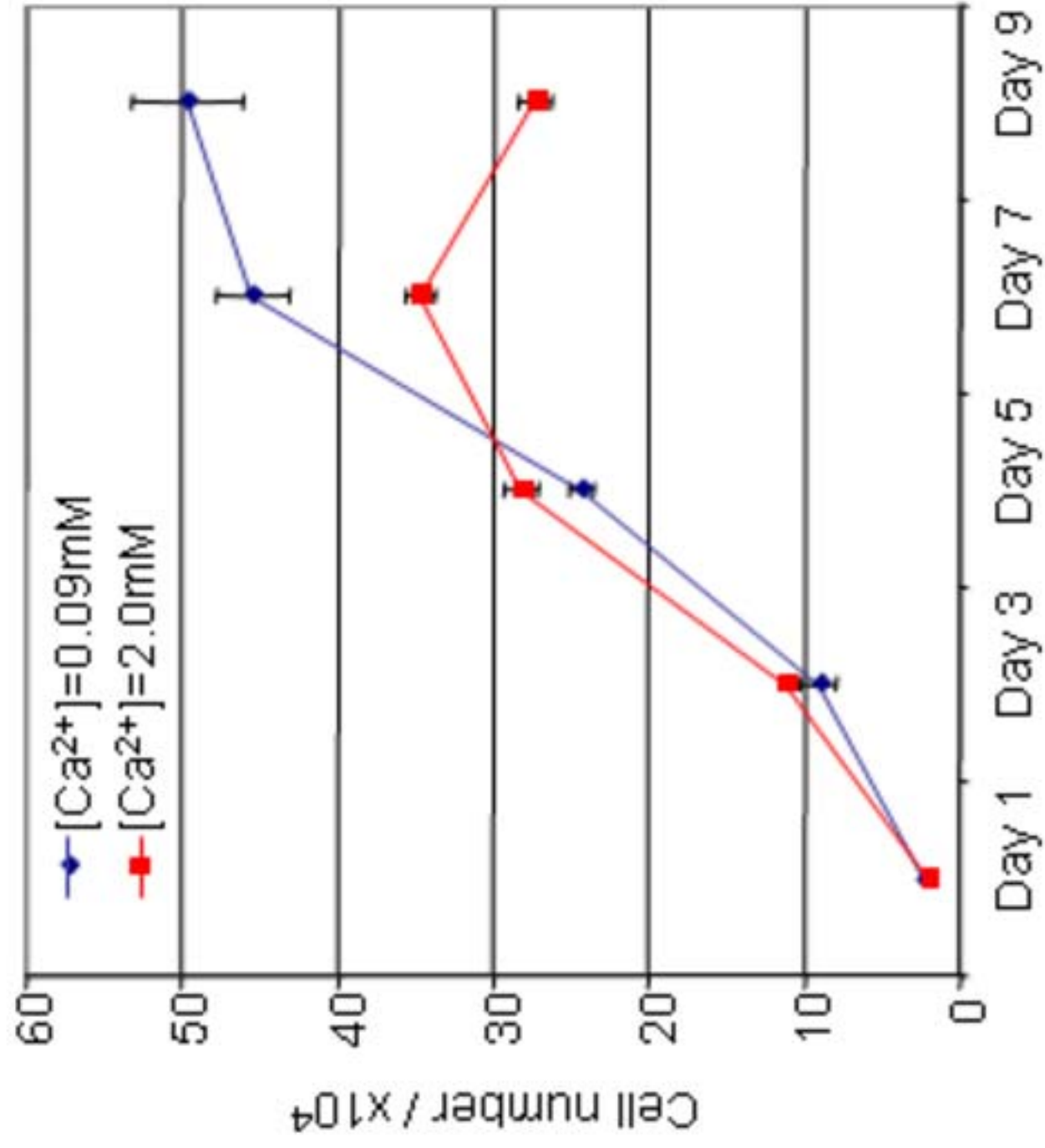
**Additional file 5**

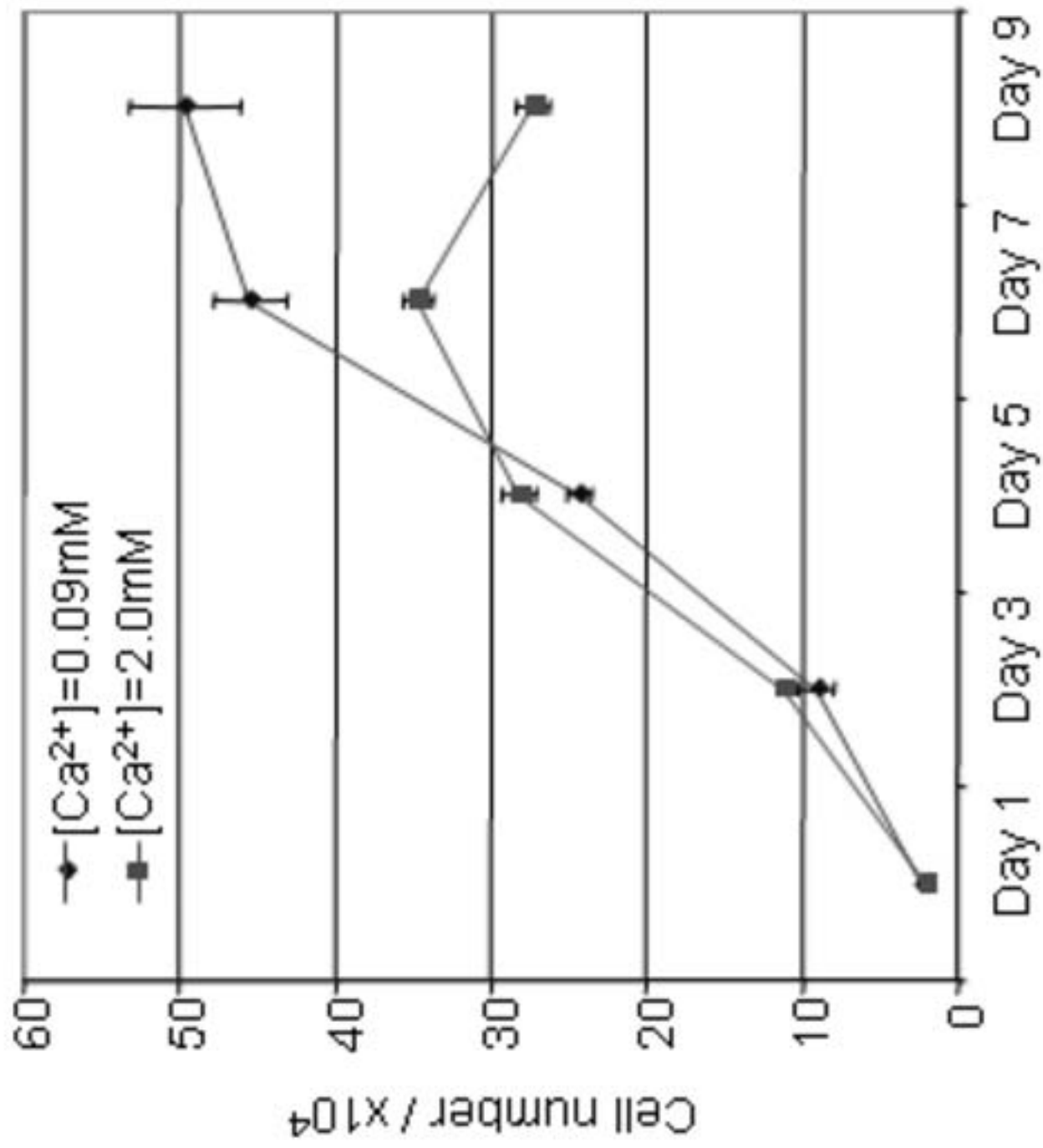
Virtual time-lapse movie of agent simulation of 100% EC-A cells in a low calcium (0.09mM) environment. Green = EC-A cells, pink = cells in M phase of cell cycle. 1 frame = 30 minutes.

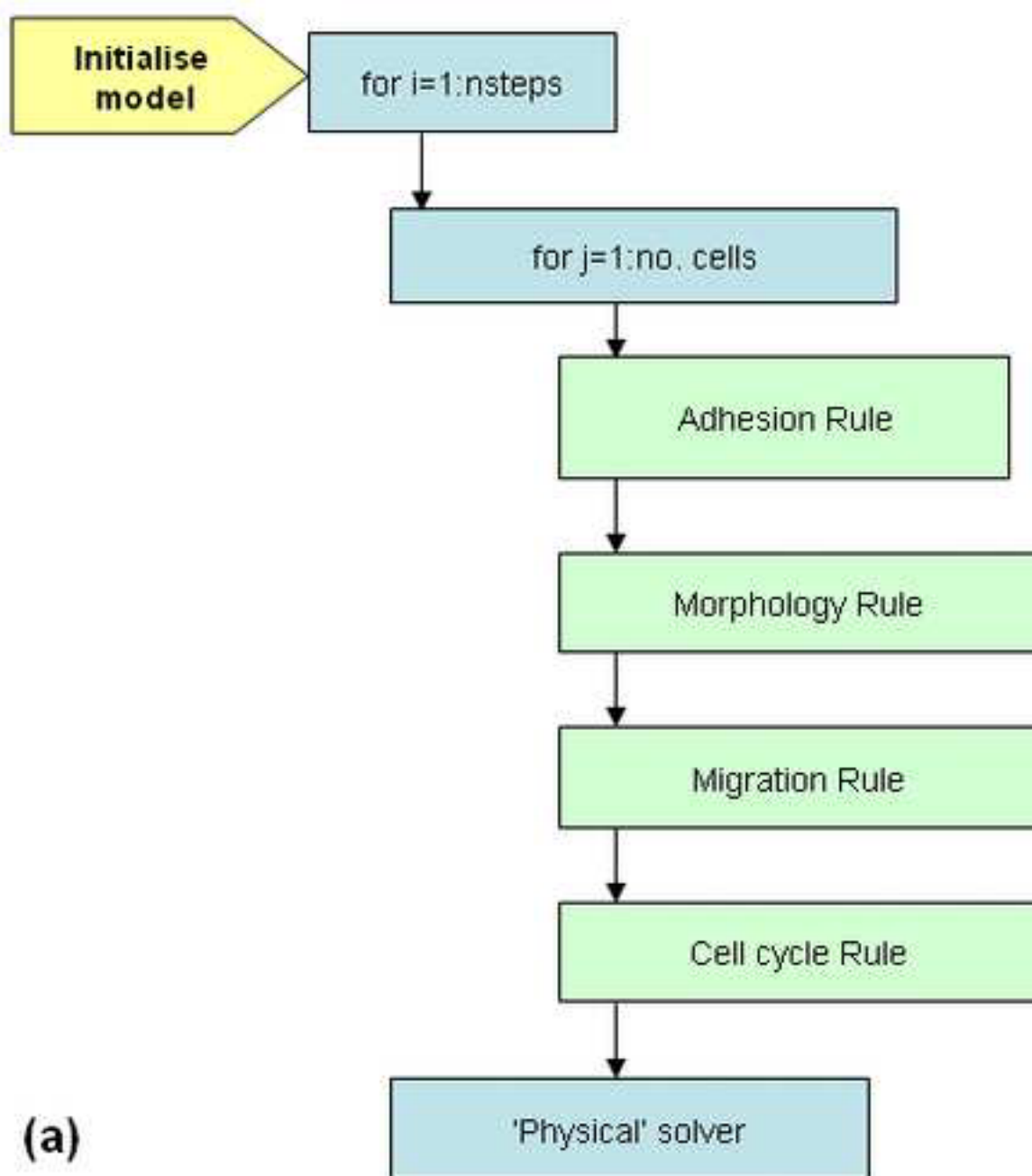
**Additional file 6**

Virtual time-lapse movie of agent simulation of 100% EC-A cells in a physiological calcium (2.0mM) environment. Green = EC-A cells, pink = cells in M phase of cell cycle. 1 frame = 30 minutes.

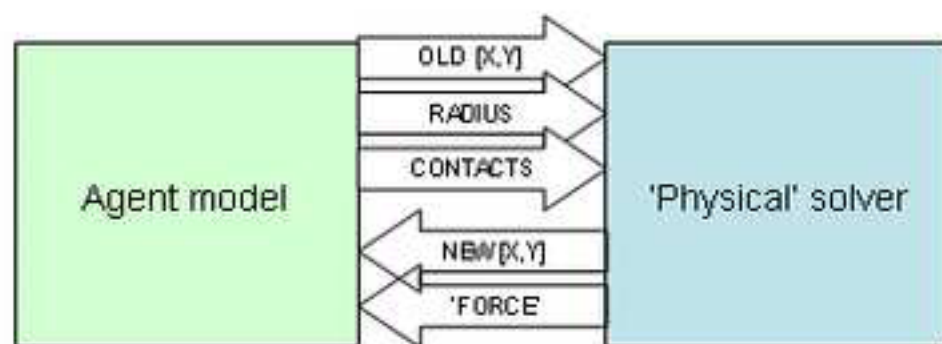
Accepted manuscript



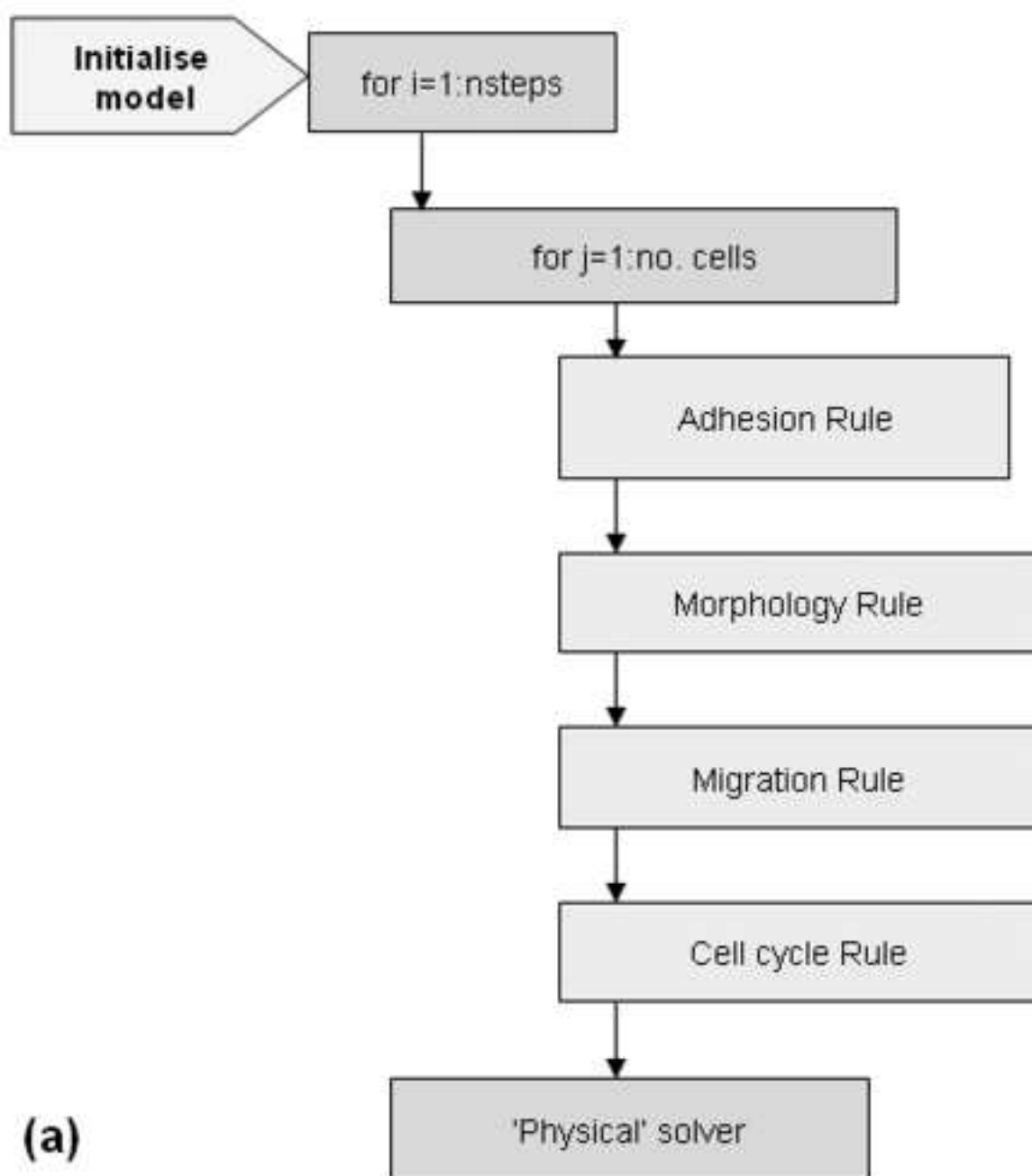




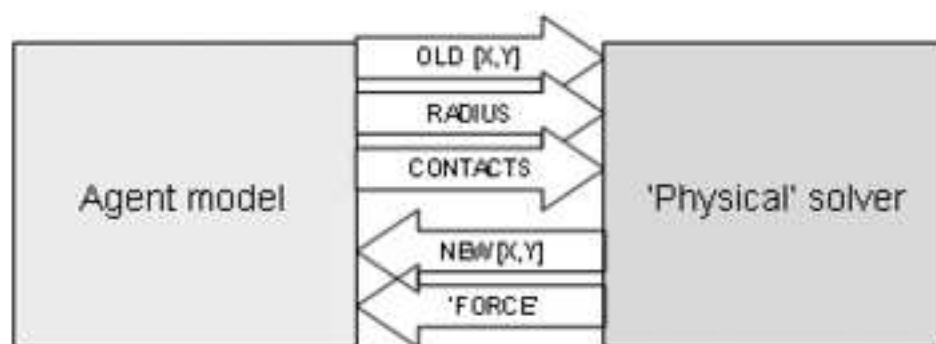
(a)



(b)



(a)



(b)

